Received: 14 November 2023 | Revised: 1 April 2024 | Accepted: 16 April 2024

DOI: 10.1002/btpr.3475

BIOTECHNOLOGY PROGRESS

RESEARCH ARTICLE

Formulation and Engineering of Biomaterials

Surface plasmon resonance aptasensing and computational analysis of *Staphylococcus aureus* IsdA surface protein

Tracy Ann Bruce-Tagoe[1] | Michael T. Harnish[2] | Shokoufeh Soleimani[3] | Najeeb Ullah[1] | Tongye Shen[2] | Michael K. Danquah[1]

[1]Department of Chemical and Biomolecular Engineering, University of Tennessee, Knoxville, Tennessee, USA

[2]Department of Biochemistry & Cellular and Molecular Biology, University of Tennessee, Knoxville, Tennessee, USA

[3]Department of Mechanical, Aerospace and Biomedical Engineering, University of Tennessee, Knoxville, Tennessee, USA

Correspondence
Michael K. Danquah, Department of Chemical and Biomolecular Engineering, University of Tennessee, Knoxville, TN 37996, USA.
Email: mdanquah@utk.edu

Funding information
National Science Foundation, Grant/Award Number: 2130658

Abstract

Staphylococcus aureus (*S. aureus*), a common foodborne pathogen, poses significant public health challenges due to its association with various infectious diseases. A key player in its pathogenicity, which is the IsdA protein, is an essential virulence factor in *S. aureus* infections. In this work, we present an integrated in-silico and experimental approach using MD simulations and surface plasmon resonance (SPR)-based aptasensing measurements to investigate *S. aureus* biorecognition via IsdA surface protein binding. SPR, a powerful real-time and label-free technique, was utilized to characterize interaction dynamics between the aptamer and IsdA protein, and MD simulations was used to characterize the stable and dynamic binding regions. By characterizing and optimizing pivotal parameters such as aptamer concentration and buffer conditions, we determined the aptamer's binding performance. Under optimal conditions of pH 7.4 and 150 mM NaCl concentration, the kinetic parameters were determined; $k_a = 3.789 \times 10^4$/Ms, $k_d = 1.798 \times 10^3$/s, and $K_D = 4.745 \times 10^{-8}$ M. The simulations revealed regions of interest in the IsdA-aptamer complex. Region I, which includes interactions between amino acid residues H106 and R107 and nucleotide residues 9G, 10U, 11G and 12U of the aptamer, had the strongest interaction, based on ΔG and B-factor values, and hence contributed the most to the stability of the interaction. Region II, which covers residue 37A reflects the dynamic nature of the interaction due to frequent contacts. The approach presents a rigorous characterization of aptamer-IsdA binding behavior, supporting the potential application of the IsdA-binding aptamer system for *S. aureus* biosensing.

KEYWORDS
aptamer, aptasensor, Bioaffinity, IsdA protein, MD simulations, *S. aureus*, surface plasmon resonance

1 | INTRODUCTION

Staphylococcus aureus (*S. aureus*), a gram-positive bacterium is a common foodborne pathogen. It is known for releasing a range of heat-resistant *staphylococcal enterotoxins* (SEs) into food, leading to the occurrence of *staphylococcal* food poisoning (SFP) in humans.[1,2] This type of food poisoning is characterized by gastroenteritis resulting from consuming contaminated food.[3] It has received significant attention due to its role as a primary cause of foodborne illness outbreaks around the world.[4] *S. aureus* has the ability to produce an extensive array of virulence factors, among them are surface proteins that are covalently linked to peptidoglycan, referred to as cell wall-anchored

(CWA) proteins.[5] The IsdA surface protein of *S. aureus*, produced in reaction to the host environment, aids colonization and decreases bacterial cell hydrophobicity, reducing the cell's ability to form biofilms. Reduction in hydrophobicity also boosts resistance to bactericidal fatty acids and peptides found in human skin. Thus, for *S. aureus* to survive in the host, the presence of IsdA is essential,[6] serving as a biomarker for the presence of the bacteria.

Within the past decades, several detection methods have been developed and used to analyze *S. aureus* in food. Prominent among which are the culture-based methods, polymerase chain reaction (PCR), immunoassays, nucleic acid-based methods and antibody-based biosensors. However, each of these methods come with their own limitations; some require lengthy procedures to generate results, others are expensive or dependent on antibodies (which have various challenges and ethical issues to produce), while others require a specific set of skills to operate, or complicated sample treatment steps.[7–9] To overcome the disadvantages of conventional methods, a new class of biosensors called aptasensors, which do not depend on antibodies but rather, aptamers are been developed.

Aptamers are short, single-stranded oligonucleotides that have the capacity to bind to or recognize their targets with high selectivity and specificity.[10,11] They can be generated for a variety of targets, through an iterative SELEX (Systematic Evolution of Ligands by Exponential Enrichment) process of selection and amplification. Aptamers are an essential part of the future of pathogen detection because they have significant advantages over the conventional antibodies. They are stable in harsh conditions and can recover their conformations when the favorable conditions are restored, they are relatively cheap and they take a shorter time to produce or modify them, they are really small which makes them easy to permeate through tissues, and they have low-to-no or minimal toxicity when used in vitro.[12–14] They also have defined structures, due to their tendency to form base pairs. They can fold into secondary structures, and then form unique three-dimensional conformations capable of specific molecular recognition of their target molecules.[15–17] Their common structural motifs are stems, hairpins, internal loops, tetraloops, purine-enriched bulges, pseudoknots, kissing complexes and G-quadruplexes conformations. These conformations are dependent on the length of the nucleic acid molecule, the primary sequence and the environmental conditions.[17,18] A nucleic acid strand has a linear sequence of nucleotide bases, with certain segments having complementary bases, that have the tendency to pair with each other, according to the Watson-Crick base-pairing rule.[19] This base pairing along the sequence forms the stem, and as the pairing occurs further along the chain, the strand loops back on itself, forming the loops and knots.[20] The G-quadruplex is one of the few structural arrangements of DNA that involves complex tertiary folding.[21] It is stabilized by the interactions of G-quartets, in which four guanines are assembled in a planar arrangement by Hoogsteen hydrogen bonding.[22,23] Aptamers have numerous applications ranging from diagnostics, therapeutics, environmental monitoring and food safety.[11,24]

Surface plasmon resonance (SPR) is an optoelectronic phenomenon that is used to monitor changes in refractive index occurring at a sensor surface.[25] This analysis serves as a powerful tool for the study of molecular interactions in real-time, without necessitating any molecular labels. At its core, SPR involves the excitation of surface plasmons, which are free electron collective oscillations, at a junction between metal and dielectric, typically gold, when it comes into contact with light at a specific angle. The plasmons are extremely sensitive to alterations in the refractive index close to the metal surface, such as when biomolecules bind or disengage from the surface. Any changes in this refractive index disrupt the resonance condition, modifying the intensity of the reflected light and thereby, enabling the tracking of molecular interactions.[26] During a typical SPR experiment, a "ligand" (one component of the interaction) is affixed to the metal surface, and the "analyte" (the other component) is passed over the surface in a flow. As the analyte binds and disengages from the ligand, the SPR signal (response unit) undergoes real-time modifications, which can be monitored to determine various kinetic properties of the interaction.[27] The interaction between a protein and an aptamer depends on the specific sequence and structure, as well as the conditions under which binding occurs. The protein-aptamer interactions involve various non-covalent interactions: hydrogen bonds between aptamer bases and protein side chains or backbone; van der Waals interaction between the aptamer and hydrophobic regions of the protein; electrostatic interactions between charged groups on the aptamer and the protein; π—π stacking between aromatic rings of the aptamer bases and aromatic side chains on the protein.[28–30] In order to achieve the design and proper functioning of advanced biosensors, such as aptasensors, knowledge on the formation process and structural basis of biomolecular complexes is necessary. The aptamer is usually prefolded to initiate target binding, providing a significant foundation for determining the complete structure.[31] Generally, the "induced-fit mechanism" is involved, which means, the structure cannot be solely inferred using conventional tools like mfold.[32,33] Moreover, most biosensing analytical tools, such as SPR, necessitate the anchoring of a biomolecule onto a surface. This immobilization process results in surface-biomolecule interactions that can lead to changes in the structure of the anchored biomolecule. Despite their significant relevance, experimental analysis of these structural alterations is often challenging to conduct, making molecular simulations a viable option to comprehend the biophysical phenomena happening at the interface between the biomolecule and the surface.[34,35] MD simulations represent a robust computational strategy that delivers critical insights into biological elements.[36,37] Through the replication of molecular interactions within a biological system, MD simulations can offer precise data regarding binding sites, structural reconfigurations, and the dynamic states of folding and unfolding of aptamers.[38,39] Furthermore, MD simulations can be employed to investigate the dynamics, architecture, and energy profiles of biological systems across various experimental scenarios, encompassing different pressures, pH levels, and temperatures.[40]

In this work, we implement SPR measurements to study the binding characteristics of a novel aptamer and the IsdA surface protein of *S. aureus* and apply MD simulations to investigate the stable and dynamic interactions of the aptamer-IsdA binding properties at the molecular level. The work also covers a parametric study of the effect of key biophysical conditions, such as pH and conductivity, on the aptamer-IsdA binding behavior. The study is targeted towards

developing a baseline binding performance to guide the implementation of the IsdA-binding aptamer, in the development of aptamers for *S. aureus* detection. The novelty of this study lies in its multifaceted approach to understanding the complexity of this specific aptamer-IsdA protein biomolecular interaction. As a premier work in this space, the study provides invaluable insights into the dynamics of this interaction, offering a foundational understanding that could significantly impact the development of theranostic tools targeting *S. aureus*. In the pursuit of detecting *S. aureus* via its IsdA protein, prior studies by Wijesinghe et al in 2023, employed a FRET-based single-molecule technique that was reported capable of detecting the foodborne pathogen protein IsdA with high sensitivity and specificity, providing meaningful findings into the potential of aptasensing in pathogen detection.[41] However, this work introduces an SPR-based aptasensing methodology, which represents a significant advancement in real-time, label-free detection. Unlike FRET-based methods, which rely on fluorescence resonance energy transfer, SPR allows for the direct observation of binding events, offering enhanced sensitivity and specificity without the need for fluorescent labeling. This eliminates potential interference from fluorescent probe photobleaching or quenching. Moreover, our approach has successfully identified two critical binding regions within the IsdA-aptamer complex, providing unprecedented detail into the interaction dynamics. These findings not only corroborate the utility of aptamers in detecting *S. aureus* but also pave the way for the development of biosensors with superior diagnostic capabilities. Further distinguishing this work is its thorough investigation into the key binding conditions (such as pH, ionic strength, and temperature) that influence the interaction between the aptamer and the IsdA protein. This comprehensive analysis sheds light on the optimal conditions for binding and contributes to a deeper understanding of the factors that govern the stability and efficacy of the aptamer-protein interaction. Such insights are crucial for the practical application of aptamers in biomedical settings, enhancing their reliability and effectiveness as biosensing elements. In addition, the construction and investigation of a molecular model to probe the binding interactions between the aptamer and the IsdA protein add a significant layer of innovation to the study. This modeling approach enables a detailed visualization and understanding of the molecular mechanisms at play, providing a framework for evaluating how variations in aptamer structure affect binding efficiency and specificity.

2 | MATERIALS AND METHODS

2.1 | Chemicals and reagents

Hepes Buffered Saline with Ethylenediaminetetraacetic Acid and Tween 20(HBS-EP$^+$) and Biotin CAPture kit, which is inclusive of Sensor chip CAP, capture reagent, and regeneration solutions were purchased from Cytiva, a subsidiary of GE Health (USA).

IsdA protein was purchased from Cusabio technology (USA) and the aptamer sequence, 5′-gcg cac gcg ugu gua gua cac acg auc gcg cgc aca auau-3′, selected against the IsdA protein in our lab via a computational SELEX approach[42] was synthesized by Integrated DNA Technologies (USA).

2.2 | Surface plasmon resonance analysis of IsdA-aptamer binding

The Biotin CAPture reagent, a blend of streptavidin and matching oligonucleotide, was utilized and integrated into the sensor chip's surface. Subsequently, the biotin-labeled aptamer (ligand) at a concentration of 500 nM was immobilized onto the sensor's surface using a running buffer (HBS-EP$^+$) at a rate of 5 μL/min over a period of 180 s. Five different concentrations of the IsdA-protein were created in the running buffer: 5000, 1667, 556, 185, and 62 nM. To begin the interaction analysis, protein samples were infused at a flow rate of 30 μL/min, starting from the lowest to the highest over a span of 180 s. Dissociation was initiated for 180 s, and the sensor surface was revitalized at 10 μL/min for 2 min. To improve the results of future cycles, an additional regeneration was introduced using 30% acetonitrile in 0.25 M NaOH solution for 2 min at 10 μL/min. After the final regeneration step, an additional rinse with the running buffer was done to cleanse the needle and flow system. The Biacore X100 evaluation software was employed to analyze the results.

2.3 | Effect of pH on IsdA-aptamer binding interaction

An acidic running buffer was prepared by adding drops of 1 M H_2SO_4 solution to the HBS-EP$^+$ buffer solution, initially at pH 7.4. The new running buffer was prepared at a pH of 4.27. 500 nM of the biotin-labeled aptamer was immobilized onto the surface of the sensor using the acidic running buffer at a rate of 5 μL/min over a period of 180 s. Five different concentrations of the IsdA-protein were created in the initially prepared HBS-EP$^+$ (pH = 7.4) running buffer: 5000, 1667, 556, 185, and 62 nM. The binding analysis was carried out using the same protocol as described earlier. A basic running buffer was prepared by adding drops of 1 M NaOH solution to the HBS-EP$^+$ buffer solution prepared at pH 7.4, to obtain a new running buffer pH of 10.4. 500 nM of the biotin-labeled aptamer was immobilized onto the surface of the sensor using the basic running buffer at a rate of 5 μL/min over a period of 180 s. Five different concentrations of the IsdA protein were prepared following the same method as the two preceding concentration series. The binding analysis was carried out using the same protocol as before.

2.4 | Effect of conductivity on IsdA-aptamer binding interaction

A new batch of five different concentrations of the IsdA-protein was prepared in the original HBS-EP$^+$ buffer (150 mM NaCl

concentration): 8000, 2667, 889, 296, and 33 nM. Binding analysis was performed using this new concentration series using the SPR protocol described earlier. 100 mL of running buffer containing NaCl concentration of 100 mM was prepared by diluting 66.7 mL of the original HBS-EP$^+$ buffer (150 mM NaCl concentration) to 100 mL with deionized water. Five different concentrations of the IsdA-protein were created in the original HBS-EP$^+$ buffer (150 mM NaCl concentration): 8000, 2667, 889, 296, and 33 nM. Binding analysis was carried out with this new low NaCl concentration-buffer using the same protocol described for the 150 mM NaCl concentration. 100 mL of running buffer containing NaCl concentration of 200 mM was prepared by dissolving 292 mg of NaCl crystals, in 100 mL of the original HBS-EP$^+$ buffer (150 mM NaCl concentration). Five different concentrations of the IsdA-protein were created in the original HBS-EP$^+$ buffer (150 mM NaCl concentration): 8000, 2667, 889, 296, and 33 nM. Binding analysis was carried out using the new high NaCl concentration-buffer using the same protocol described for the 150 mM NaCl concentration.

2.5 | Computational studies

MD simulations of the aptamer-IsdA protein interaction were performed using the AMBER20 software suite. The initial coordinates of the IsdA protein were obtained from the rcsb website (PDB 2O1A) and the aptamer structure was modeled using ROSETTA. Haddock was used to create the IsdA protein-aptamer complex structure and a docking model was chosen, based on the scoring function. The initial topology and coordinate files were generated using the program LEAP from the AMBER20 tool suite. AMBER force fields were used, including RNA.Shaw for the aptamer and protein.ff19SB for the protein. Additionally, TIP3P water was used for solvating the system and 34 counter ions (Na^+) were used to neutralize the system. NAMD was utilized for minimization and heating to equilibrate the system, and to conduct the simulations. Energy minimization was conducted in two phases; first, the solvent and ions were minimized while restraining the solute, followed by minimization of the entire system without restraints. The system was heated gradually from 0 to 300 K over 100 ps using the Langevin thermostat with a collision frequency of 1.0/ps. Positional restraints were applied to the protein and aptamer with a force constant of 2 kcal/mol/Å^2, to maintain structural integrity during heating. The equilibration phase was carried out under NPT conditions (statistical ensemble in MD simulations where the Number of particles (N), Pressure (P), and Temperature (T) of the system are held constant[43]) for 1 ns to adjust the density and pressure of the system, with the Berendsen barostat employed to maintain 1 atm pressure. Production runs were performed under the NPT ensemble at 300 K and 1 atm for 100 ns. Data was collected every 500 time steps (1 ps interval). In total, 100,000 frames of data were collected. At an interval of 10 ps, root mean square deviation (RMSD) and b-factor were calculated to characterize the fluctuation and flexibility of the molecules. A lower frequency of per 100 ps was used for MM/GBSA calculation, which was performed to reveal the molecular binding interaction. Data visualization and further statistical analysis were performed using VMD and xmgrace, respectively. All simulations were conducted on the Stampede2 supercomputer at the Texas Advanced Computing Center (TACC).

3 | RESULTS AND DISCUSSION

3.1 | Computational analysis of the aptamer-IsdA protein interaction

After the analysis of the interaction, it was observed that the complex had both stable and dynamic parts contributing to the binding. The map in Figure 1 defines a contact as any part of a residue coming within 4.2 Å with any part of another residue. This is a typical cutoff for considering whether two residues are in close proximity to suggest a significant interaction.[44] This contact map provides a visual representation of where and how the aptamer interacts with the protein, which is crucial for understanding the molecular basis of their binding and function. The circled regions are of particular interest for studying the structural dynamics of the complex or modifying the protein or the aptamer for improved interaction characteristics.

In Figure 1b, the interactions between the IsdA protein and the aptamer are displayed. The clusters of points represent key areas where the aptamer binds to the protein. There are two regions that provide major contributions to the stability and dynamic binding of the complex. Region I has the strongest interaction, which contains the residues with the most negative ΔG values (such as those between protein H106/R107 and aptamer 9G, 10U, and 11G) and the lowest B-factor values for the aptamer (10U, 11G, 12U). These two factors create a high affinity and highly stable interface. The close proximity of the points in this region indicates a strong and potentially stable interaction between specific aptamer and IsdA protein regions, possibly due to a greater number of hydrogen bonds, van der Waals interactions, or electrostatic attractions. Multiple interactions often lead to increased binding strength. The specificity of the interaction can be inferred from the particular residues that interact. A tight cluster of interactions indicates that only specific parts of the aptamer and protein are involved in binding.[28] These specific parts include protein H106/R107 and in the aptamer 9G, 10U, and 11G.

Region II is smaller and has less dense contact points and a weaker interaction. This Region II involves important amino acid residues K116, A117, P119 and T120 and nucleotide residues 36A, 37A, 38U at the 3′ end of the aptamer. However, it still exhibits frequent contact with relatively high stability. The sparser interactions in region II may reflect the dynamic nature of the interaction, with the potential for conformational changes in the protein or aptamer upon binding or release.

A third interaction region, Region III, involving the portion of the aptamer that is highly flexible and contributes to repulsive interaction

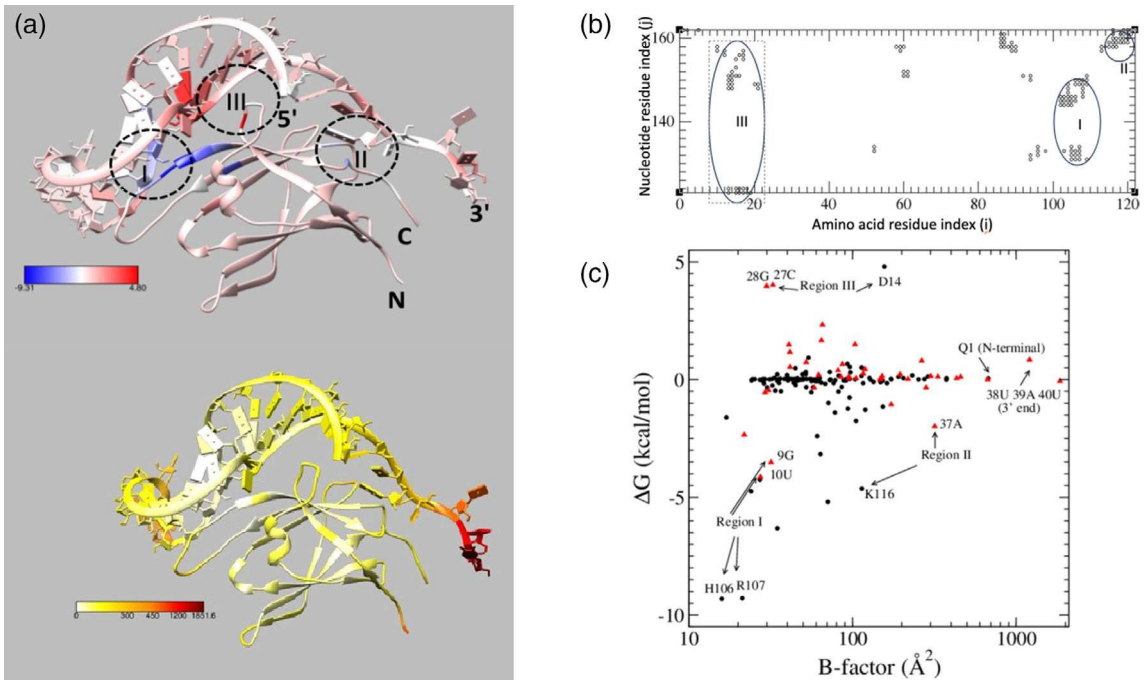

FIGURE 1 (a) 3D cartoon representation of protein-aptamer complex is color-coded by interaction (upper) and B-factor (lower). Three important regions are labeled, where Regions I and II provide attractive interaction and major contributions to the stability of the complex, whereas Region III is strongly repulsive and provides instability and contributes to the fast kinetic nature of this association. (b) The mean contact interaction map between protein (1–122) and RNA (40 nt, internal index 123–162). Here each circle indicates a significant contact between an amino acid residue and a nucleotide residue. A contact is considered significant if the corresponding instant contact is formed at least 10% during the simulation. Near diagonal contacts (between residues N and N + 1/N + 2) have been removed. Three important regions are annotated with ovals. (c) Scatter plot depicting per-residue ΔG versus B-factor. Labeled residues include selected residues with meaningful contributions to contacts within region I, region II, and the flexible aptamer region.

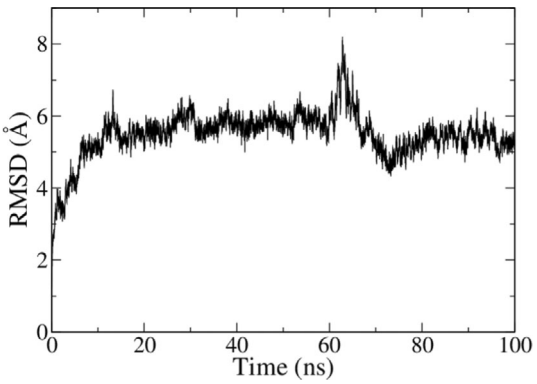

FIGURE 2 The root mean square deviation (RMSD) of the IsdA protein-RNA aptamer complex as a function of time. The overall translation and rotation degrees of freedom were removed by fitting each frame to the first frame of the simulation. The complex stabilized after the initial 10 ns of the simulation.

(positive ΔG), which also contributes to fast association and dissociation rates.

The RMSD plot shows the changes in the conformation of the IsdA protein-aptamer complex over the course of a 100 ns MD simulation. RMSD is a commonly used measure to determine the stability of protein-ligand complexes over time in a simulation. The RMSD increases sharply at the beginning (first 10 ns), which is typical, as the system departs from the initial structure and settles into a more energetically favorable conformation. This period often includes the relaxation of any strained bonds or unfavorable interactions present in the starting model. After the initial rise, the RMSD fluctuates, which indicates that the complex is exploring conformational space. These fluctuations are a normal part of the simulation as the complex experience various intermolecular interactions and thermal motion. The peak around 60 ns suggests a transient conformational change or a period of increased flexibility within the complex. This could be due to the protein or aptamer reaching a state of high energy before settling into a more stable configuration. Following the peak, the RMSD decreases and stabilizes, which implies that the complex has found a more stable conformation compared to the state at 60 ns. The downward trend suggests a relaxation from the peak conformation back to a more stable state. Towards the end of the simulation, the RMSD appears to plateau, suggesting that the complex has reached a relatively stable conformation. This plateau indicates that most of the major conformational changes have occurred and the system has equilibrated. Figure 2 explains the RMSD of the IsdA protein-RNA aptamer complex as a function of time. The overall translation and rotation degrees of freedom were removed by fitting each frame to the first frame of the simulation. The complex stabilized after the initial 10 ns of the simulation.

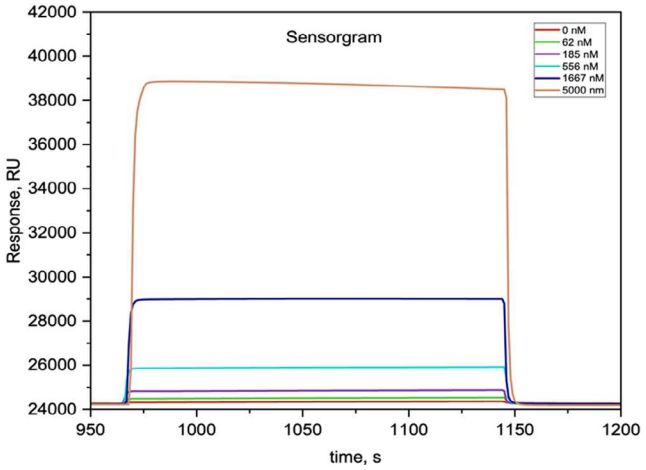

FIGURE 3 Surface plasmon resonance (SPR) sensorgram generated from the interaction in a buffer of neutral pH conditions. The analysis was carried out at 25°C and a pH of 7.4, for different concentrations of IsdA protein between 0 and 5000 nM, indicated by the different colored curves.

The degree of fluctuation in RMSD reflects the conformational flexibility of the complex. Moderate fluctuations suggest that while the complex is generally stable, there are dynamic regions that allow for some movement, which may be important for biological function. An RMSD which is stabilized at lower values demonstrates a tight binding affinity and high specificity, because the complex does not deviate much from its preferred structure. The plot does not show excessively high RMSD values, which suggests the complex is reasonably stable, a desirable feature for strong and specific binding interactions.

3.2 | SPR analysis of the aptamer-IsdA protein interaction

The results of the SPR analysis are given in a sensorgram, which is a graph of response in RU versus time in seconds. Different concentrations were analyzed in different cycles and these are indicated in different colors on the graph.

During each of the analysis cycles, analyzed at pH 7.4, the achieved level of aptamer immobilization was in a narrow range of 24,200–24,300 Response Units (RU), attributable to the constant aptamer concentration on the same sensor chip used for the analysis.

Under physiological conditions (pH of 7.4), the ionizable groups on both the IsdA and aptamer would have specific charges that will influence the binding interaction. The aspartic acid (Asp, D) and glutamic acid (Glu, E) residues in the IsdA would be deprotonated and carry a negative charge while the lysine and arginine residues would be protonated depending on its local environment.[45] Nucleic acid aptamers are polyanionic due to their phosphate backbone. These phosphate groups will be deprotonated and negatively charged.[46] The aptamer bases also participate in hydrogen bonding and π—π stacking interactions with the amino acid side chains and aromatic residues of the IsdA, like phenylamine, tyrosine and tryptophan.[28,29] The negatively charged phosphate backbone of the aptamer interacts with the positively charged regions on IsdA such as the Lys and Arg residues, forming salt bridges.[10] The b-factor and MM/GBSA analysis revealed the section of the residues forming the salt bridges as region 1, which consists of histidine and arginine. From the simulation, we can observe that these salt bridges are the ones contributing mostly to the stable interaction between the aptamer and IsdA protein, due to the low b-factor values and strong attractive energy contributions obtained in this region.

Figure 3, shows the SPR sensorgram curves corresponding to the varying analyte concentrations. As anticipated, the least response unit was observed with the lowest concentration sample and vice versa, confirming a stable and tight binding behavior of the IsdA protein to the immobilized aptamer. The immobilized aptamer on the chip surface presents adequate binding sites that allowed for the binding of protein molecules even at an increasing concentration below the maximum binding capacity. This finding also underscores the crucial role of concentration in the binding analysis. Utilizing a straightforward 1:1 kinetic model, allowed us to fit the interaction data, resulting in the evaluation of important kinetic parameters. The association, dissociation, and equilibrium dissociation constants were determined to be $k_a = 3.789 \times 10^4$/Ms, $k_d = 1.798 \times 10^{-3}$/s, and $K_D = 4.745 \times 10^{-8}$ M, respectively. The model used in this analysis is similar to the one used by Sun et al. (2021), where they analyzed the binding-induced SPR signals and obtained the sensitive detection of NSE and ProGRP31-98. They were able to analyze the kinetic parameters associated with the interaction and obtained detection limits of 3.9 nM for NSE and 15.6 nM for ProGRP31-98.[47] The results were also quite similar in the context of the specific target molecules used in each research. This result demonstrates good binding stability and affinity to the IsdA protein. The K_D value represents the molar concentration of the aptamer needed to bind to half of the active sites of the IsdA protein. The fact that the K_D value is low suggests a high level of affinity of the aptamer to IsdA, implying that even minute amounts of the aptamer demonstrate affinity to IsdA. It also shows that the complex is quite stable. This outcome is consistent with the simulation results. Stable RMSD at lower values is indicative of a tight binding affinity and high specificity, as it suggests that the complex does not deviate significantly from a preferred conformation. The plot obtained from the simulation did not show high RMSD values and the fluctuations were moderate, which signals that the complex is fairly stable. However, the k_a and k_d values from the SPR reflect fast kinetics, which indicates significant flexibility in the structure of the complex. This observation can be supported by the flexible nature of the third region, that is the region between regions 1 and 2, discovered through the simulation. To attribute the SPR changes specifically to the interaction between the aptamer and the IsdA protein, we conducted control experiments using N-protein as non-specific analytes. The controls were matched in refractive index to the solutions containing the IsdA protein with no biomolecular interaction. We compared the SPR changes in these control experiments to those

TABLE 1 Kinetic Parameters evaluated at different pH conditions.

pH	K_a /Ms	K_d /s	K_D, M
4.27	20.24	3.465×10^{-2}	1.712×10^{-3}
7.4	3.789×10^{4}	1.798×10^{-3}	4.745×10^{-8}
10.4	3224	4.001×10^{-2}	1.241×10^{-5}

observed in the presence of IsdA protein and were able to isolate the effects of refractive index changes due to the specific binding events. In addition, we utilized a kinetic analysis approach to directly assess the impact of interaction dynamics on the SPR signal. We monitored the SPR changes over time and captured the real-time binding kinetics between the aptamer and the IsdA protein. This method allowed us to distinguish between the initial refractive index changes, which occur upon solution exchange at the sensor interface, and the subsequent changes that are indicative of the specific binding events. Table 1 shows Kinetic Parameters evaluated at different pH conditions.

3.2.1 | Effects of pH on the interaction between IsdA protein and aptamer

Figure 4a shows the binding results at pH 4.27. The sensorgram shows an immobilization response of 26,600–26,670 Response Units (RU), a significant increase from the immobilization level recorded in the neutral buffer. At a pH of 4.27, the ionization states of several amino acid side chains and the aptamer's phosphate backbone can be affected, which in turn influences the binding interaction. A significant portion of the acidic residues of IsdA; Asp (pKa = 4.0) and Glu (pKa = 4.4) are protonated, becoming closer to electrical neutrality. While, the basic residues; Lysine (Lys, K), Arginine (Arg, R) with pKa of 10.5 and 12.5, respectively, remain protonated and positively charged. Histidine (His, H), with a pKa around 6.0 will be predominantly protonated and positively charged. The phosphate backbone of the aptamer will still be deprotonated and negative, but the degree of the charge couple potentially reduces slightly, due to the proximity to pKa values of the phosphodiester linkage. This may cause a change in the stability of the conformation of the aptamer. The nature of electrostatic interactions shifts, due to the changes in the charge distribution of the protein. Specifically, regions that were previously negatively charged due to Asp and Glu, becoming closer to electrical neutrality. However, the protonation of His enhances certain interactions with the aptamer. Protonated histidine can participate in hydrogen bonding more effectively and increase the positive charge on the protein, which strengthens electrostatic interactions with negatively charged regions on the aptamer. The shift in pH from 7.4 to 4.27 can reduce the combination of hydrogen Bonding, electrostatic Interactions and disrupt salt bridges, significantly altering the overall binding affinity. Throughout the different cycles, the response recorded was quite higher than that recorded in the neutral region. However, it yielded far less interaction in comparison to what occurred in the neutral region. In the kinetic analysis, the association rate constant, k_a was evaluated as 20.24/Ms, which shows a very low rate of complex formation. Looking at the dissociation rate constant, k_d of 3.465×10^{-2}/s, we notice that the dissociation occurred faster than it did in the neutral region. This means a higher degree of complex dissociation per unit second. The fact that the response units were relatively high, but did not reflect in the kinetic parameters could be associated with the fast dissociation rate, causing the reaction to proceed too quickly to record stable values. This can even be seen in the fact that the time frame for the reaction in this case was somewhat shorter than in the neutral region. Also, the equilibrium dissociation constant obtained was 1.712×10^{-3} M, equivalent to 1.712 mM. This value shows that the binding affinity was very low, and could be associated with the denaturing of the IsdA protein at the low pH, since proteins are typically sensitive and are easily denatured.

Figure 4b shows the interaction results in a basic buffer system, at pH 10.4. From the sensorgram, an immobilization response of 26,230–26,250 Response Units (RU) was obtained, an increase from the immobilization level recorded in the neutral buffer, but lower than the immobilization level in the acidic environment.

At a pH of 10.4, the acidic residues of IsdA are deprotonated and negatively charged. Some Lys residues will deprotonate leaving most of the Lys residues still positively charged. Arg remains positively charged and His is mostly deprotonated and neutral. The phosphate backbone of the aptamer would remain as it was in the physiological pH. Generally, at a pH of 10.4 the IsdA protein and aptamer structures are similar to what they were at a pH of 7.4. Hence, there will be a good π—π stacking, hydrogen bonding and van der Waals interaction, with a reduction in certain electrostatic interactions due to the deprotonated Lys.

This is consistent with the results when the responses are compared to that of the neutral and acidic buffer throughout the different cycles. Overall, the interaction was better in the basic buffer than it was in the acidic buffer, but not as good as in the neutral buffer. This can be seen in the kinetic evaluation results; $k_a = 3224$/Ms, $k_d = 4.001 \times 10^{-2}$/s and $K_D = 1.241 \times 10^{-5}$. From the kinetic results we notice that the complex formed at a significantly higher rate than it did in the acidic buffer, so even though the dissociation rate was higher, indicative of less favorable interaction kinetics at higher pH, the affinity was better, due to the fact that the complex was formed a lot faster than it separated, giving enough time for interaction to be recorded. The K_D recorded still indicates a relatively strong interaction, indicating that the aptasensor could potentially be functional across a range of pH values, although with decreased efficiency at high pH levels.

3.3 | Effect of conductivity on the interaction between IsdA protein and aptamer

Three different experiments were conducted, keeping all other parameters constant and varying salt concentration in the running buffer. The first experiment was based on normal running buffer purchased from the manufacturer, which contains 150 mM NaCl salt, and in the

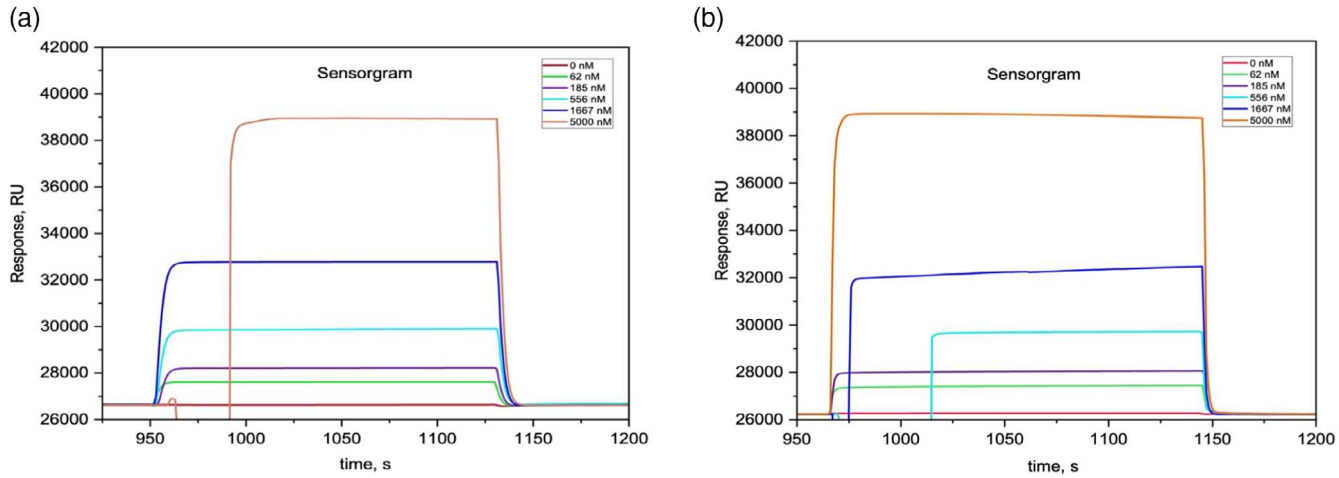

FIGURE 4 Surface plasmon resonance (SPR) Sensorgram generated from the interaction in running buffer containing sulfuric acid. The analysis was carried out at 25°C and varying pH, for different concentrations of IsdA protein between 0 and 5000 nM. (a) Interaction results at a pH of 4.27, (b) interaction results at a pH of 10.4.

NaCl concentration, mM	K_a /Ms	K_d /s	K_D, M
100	3.045×10^5	2.447×10^{-3}	8.036×10^{-9}
150	1.001×10^5	5.996×10^{-4}	5.991×10^{-9}
200	8.181×10^4	9.747×10^{-4}	1.192×10^{-8}

TABLE 2 Kinetic Parameters evaluated at different ironic strengths.

other two experiments, the salt concentration was changed to 100 and 200 mM, respectively to study the effect of conductivity on binding. The presence of NaCl in the buffer introduces additional ions into the solution, which can influence the chemistry of binding between the IsdA and aptamer. The structure of the protein and aptamer could be altered by the increased ironic strength. The ironic strength of the solution has an effect on the Debye length, which is a parameter that describes the effective range of electrostatic interactions in the solution.[48] When the magnitude of this length is small, it implies that the species need to be closer together to have significant electrostatic interactions and vice versa. In the buffer containing 150 mM NaCl, the Debye length would be shorter, leading to weaker long-range electrostatic interactions compared to a buffer with lower ironic strength. The Na^+ and Cl^- ions can shield the charges on the charged residues of the IsdA and aptamer, reducing the significant electrostatic interactions.[49,50] Conversely, the presence of salts decreases non-specific binding through the increase in "charge screening."

The results of the first experiment at 150 mM showed the kinetic parameters; $k_a = 1.001 \times 10^5$/Ms, $k_d = 5.996 \times 10^{-4}$/s and $K_D = 5.991 \times 10^{-9}$ M. From these results, we see that, 150 mM NaCl concentration is enough to maintain a good binding interaction without shielding the charges on the protein and aptamer to prevent electrostatic binding. Table 2 shows Kinetic Parameters evaluated at different ironic strengths.

The k_a obtained from the binding in the running buffer containing 100 mM NaCl is significantly higher (3.045×10^5/Ms) than in the normal buffer (1.001×10^5/Ms). This suggests that the presence of a lower salt concentration enhances the binding interactions between the IsdA protein and its aptamer, leading to a faster formation of the complex. This can be explained by an increase in Debye length caused by a decrease in ironic strength. This leads to more significant long-range electrostatic interactions, because charged particles do not have to be very close to form bonds. There are only a few irons preventing the negatively charged phosphate backbone from binding to the positively charged residues on the IsdA protein. Since the IsdA-aptamer binding is largely driven by electrostatic interactions, a higher association rate is recorded. The increase in non-specific binding with decreased ironic strength explains why the second analysis recorded k_d (2.447×10^{-3}/s) is relatively higher, compared to the 150 mM NaCl buffer (5.996×10^{-4}/s), indicating that the complex formed in the low salt buffer is less stable and more prone to dissociation. Non-specific bonds are weaker and easily disrupted hence, they dissociate at a faster rate. K_D in the running buffer containing 100 mM NaCl (8.036×10^{-9}) is higher than in the normal buffer (5.991×10^{-9}). A higher K_D value suggests a weaker binding affinity in the lower salt buffer, indicating that the interaction is weak and the complex is less stable compared.

The decrease in binding affinity observed in the low salt buffer is in line with the known effect of decreasing ionic strength on electrostatic interactions between molecules.

The k_a value recorded based on the 200 mM salt buffer (8.181×10^4/Ms) is notably lower than in the normal running buffer (1.001×10^5/Ms), suggesting that the presence of a higher salt concentration weakens the binding interactions between the IsdA protein and its aptamer, which lead to a slower formation of the

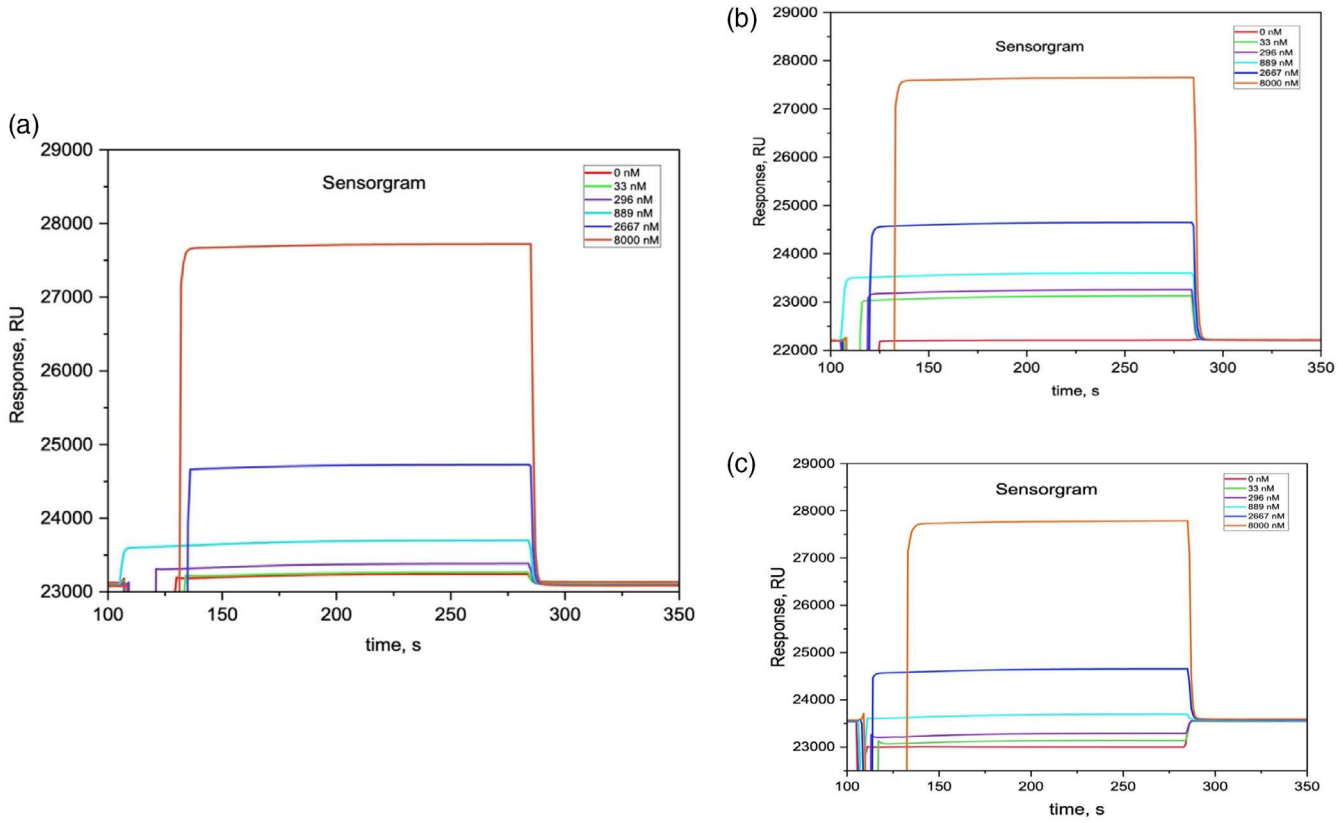

FIGURE 5 Surface plasmon resonance (SPR) Sensorgram generated from the interaction in various salt concentrations (150 mM NaCl). The analysis was carried out at 25°C, for different concentrations of IsdA protein between 0 and 8000 nM. (a) results for running buffer containing 150 mM NaCl, (b) results for running buffer containing 100 mM NaCl, (c) results for running buffer containing 200 mM NaCl.

complex. The k_d (9.747×10^{-4}/s) is also higher compared to the normal running buffer (5.996×10^{-4}/s), showing how the complex formed in the 200 mM salt buffer is less stable and more prone to dissociation. K_D (1.192×10^{-8} M) is substantially higher than in the normal buffer (5.991×10^{-9} M), indicating that the aptamer has a lower binding affinity towards the IsdA in a high ironic environment. This decrease in binding affinity seen in the high salt concentration buffer is consistent with the literature, which reports the effect of increasing ionic strength on electrostatic interactions. As the ionic strength increases, the significance of electrostatic interactions in the binding mechanism would generally diminish due to increased charge shielding.[49] The sensorgram also shows the low binding interaction at IsdA protein concentrations below 800 nM. Figure 5 explains SPR Sensorgram generated from the interaction in various salt concentrations (150 mM NaCl). The analysis was carried out at 25°C, for different concentrations of IsdA protein between 0 and 8000 nM. (a) results for running buffer containing 150 mM NaCl, (b) results for running buffer containing 100 mM NaCl, (c) results for running buffer containing 200 mM NaCl.

4 | CONCLUSION

This work utilized both computational and experimental methods to probe the nature of the interaction between an IsdA-binding aptamer and IsdA protein. The findings from this work shows that the aptamer sequence selected, forms a stable complex with the IsdA protein, indicating that it has a good affinity towards the IsdA protein and can be used as a biosensor probe for detecting IsdA. The computational results revealed some insight into both stable and dynamic binding regions in the complex and the experimental results provided details into the kinetics of the interaction. The work also shows that binding kinetics and stability of the IsdA protein-aptamer interaction are significantly influenced by changes in pH and ironic strength (conductivity). Analysis under different pH conditions yielded K_D values of 1.712×10^{-3}, 4.745×10^{-8} and 1.241×10^{-5} M, for pH values of 4.27, 7.4 and 10.4, respectively. These results can be associated with the overall interaction contribution from electrostatic, π—π stacking, hydrogen bonding and van der Waals interactions. The B-factor and energy calculations showed that IsdA residues H106/R107 and aptamer 9G, 10U, and 11G contributed to stable binding in Region I; while aptamer residues 36A, 37A, 38U and IsdA residues K116, A117, P119 and T120 contributed to the binding in Region II. And finally, interactions between residues 27C/28G and D14 of Region III contributed to the flexibility of the complex. This flexibility explains the fast k_{on} and k_{off} obtained from the SPR data. The low RMSD values and the moderate fluctuations observed in the RMSD plot indicates stability in the aptamer-IsdA complex. Comparing the experimental and computational results show how MD

simulations can be used to validate the experimental results based on conformational states and specific binding sites. This work also demonstrates the importance of carefully controlling the buffer conditions in SPR experiments. Different pH and salt concentrations (ionic strength) can alter the binding behavior, and it is essential to optimize the binding conditions to obtain the best signal output in biosensing applications. Understanding the structural mechanism of the biomolecular complex formation and the effects of pH and ionic strength on biomolecular interactions, can aid in the design of more effective detection strategies and provide insights into the regulation of molecular interactions in biological systems.

AUTHOR CONTRIBUTIONS

Tracy Ann Bruce-Tagoe: Investigation; methodology; writing – original draft; formal analysis; data curation. **Michael T. Harnish:** Software; data curation. **Shokoufeh Soleimani:** Writing – review and editing; visualization. **Najeeb Ullah:** Writing – review and editing; validation. **Tongye Shen:** Software; supervision. **Michael K. Danquah:** Conceptualization; funding acquisition; project administration; supervision; resources.

ACKNOWLEDGMENTS

The authors wish to acknowledge the financial support from the National Science Foundation (Grant # 2130658). The simulation work performed on Stampede2 at TACC through allocation MCB120011 from the Advanced Cyberinfrastructure Coordination Ecosystem: Services & Support (ACCESS) program, which is supported by National Science Foundation.

CONFLICT OF INTEREST STATEMENT

The authors declare no conflicts of interest.

DATA AVAILABILITY STATEMENT

The data that support the findings of this study are available from the corresponding author upon reasonable request.

ORCID

Michael K. Danquah https://orcid.org/0000-0002-4232-7138

REFERENCES

1. Oliveira D, Borges A, Simões M. *Staphylococcus aureus* toxins and their molecular activity in infectious diseases. *Toxins*. 2018;10(6):252. doi:10.3390/TOXINS10060252
2. Wang W, Baloch Z, Jiang T, et al. Enterotoxigenicity and antimicrobial resistance of *Staphylococcus aureus* isolated from retail food in China. *Front Microbiol*. 2017;8:294544. doi:10.3389/FMICB.2017.02256/BIBTEX
3. Lv GP, Xu BH, Wei PN, et al. Molecular characterization of foodborne-associated *Staphylococcus aureus* strains isolated in Shijiazhuang, China, from 2010 to 2012. *Diagn Microbiol Infect Dis*. 2014;78(4):462-468. doi:10.1016/J.DIAGMICROBIO.2013.12.006
4. Wu S, Duan N, Gu H, et al. A review of the methods for detection of *Staphylococcus aureus* enterotoxins. *Toxins*. 2016;8(7):176. doi:10.3390/TOXINS8070176
5. Foster TJ, Geoghegan JA, Ganesh VK, Höök M. Adhesion, invasion and evasion: the many functions of the surface proteins of *Staphylococcus aureus*. *Nat Rev Microbiol*. 2013;12(1):49-62. doi:10.1038/nrmicro3161
6. Clarke SR, Mohamed R, Bian L, et al. The *Staphylococcus aureus* surface protein IsdA mediates resistance to innate defenses of human skin. *Cell Host Microbe*. 2007;1(3):199-212. doi:10.1016/J.CHOM.2007.04.005
7. Gao D, Ma Z, Jiang Y. Recent advances in microfluidic devices for foodborne pathogens detection. *TrAC – Trends Anal Chem*. 2022;157:116788. doi:10.1016/J.TRAC.2022.116788
8. Zaid MHM, Saidykhan J, Abdullah J. Nanosensors based detection of foodborne pathogens. *Nanotechnol: Appl Energy Drug Food*. 2019;377-422. doi:10.1007/978-3-319-99602-8_19/FIGURES/30
9. Bioaffinity M, Ann Bruce-Tagoe T, Danquah MK. Bioaffinity nanoprobes for foodborne pathogen sensing. *Micromachines*. 2023;14(6):1122. doi:10.3390/MI14061122
10. Adachi T, Nakamura Y. Aptamers: a review of their chemical properties and modifications for therapeutic application. *Molecules*. 2019;24(23):4229. doi:10.3390/MOLECULES24234229
11. Chandola C, Kalme S, Casteleijn MG, Urtti A, Neerathilingam M. Application of aptamers in diagnostics, drug-delivery and imaging. *J Biosci*. 2016;41(3):535-561. doi:10.1007/S12038-016-9632-Y
12. Banu K, Mondal B, Rai B, Monica N, Hanumegowda R. Prospects for the application of aptamer based assay platforms in pathogen detection. *Biocybern Biomed Eng*. 2022;42(3):934-949. doi:10.1016/J.BBE.2022.07.005
13. Byun J. Recent Progress and opportunities for nucleic acid aptamers. *Life*. 2021;11(3):193. doi:10.3390/LIFE11030193
14. Liu Q, Zhang W, Chen S, et al. SELEX tool: a novel and convenient gel-based diffusion method for monitoring of aptamer-target binding. *J Biol Eng*. 2020;14(1):1-13. doi:10.1186/S13036-019-0223-Y/FIGURES/7
15. Yoo H, Jo H, Oh SS. Detection and beyond: challenges and advances in aptamer-based biosensors. *Mater Adv*. 2020;1(8):2663-2687. doi:10.1039/D0MA00639D
16. Wang QL, Cui HF, Du JF, Lv QY, Song X. In silico post-SELEX screening and experimental characterizations for acquisition of high affinity DNA aptamers against carcinoembryonic antigen. *RSC Adv*. 2019;9(11):6328-6334. doi:10.1039/C8RA10163A
17. Zhou J, Rossi J. Aptamers as targeted therapeutics: current potential and challenges. *Nat Rev Drug Discov*. 2017;16(3):181-202. doi:10.1038/NRD.2016.199
18. Mascini M, Palchetti I, Tombelli S. Nucleic acid and peptide aptamers: fundamentals and bioanalytical aspects. *Angew Chem Int Ed*. 2012;51(6):1316-1332. doi:10.1002/ANIE.201006630
19. Takahashi S, Sugimoto N. Watson-crick versus Hoogsteen Base pairs: chemical strategy to encode and express genetic information in life. *Acc Chem Res*. 2021;54(9):2110-2120. doi:10.1021/ACS.ACCOUNTS.0C00734/ASSET/IMAGES/LARGE/AR0C00734_0007.JPEG
20. Tok JBH, Cho J, Rando RR. RNA aptamers that specifically bind to a 16S ribosomal RNA decoding region construct. *Nucleic Acids Res*. 2000;28(15):2902-2910. doi:10.1093/NAR/28.15.2902
21. Tucker WO, Shum KT, Tanner JA. G-quadruplex DNA aptamers and their ligands: structure, function and application. *Curr Pharm Des*. 2012;18(14):2014-2026. doi:10.2174/138161212799958477
22. Gatto B, Palumbo M, Sissi C. Nucleic acid aptamers based on the G-quadruplex structure: therapeutic and diagnostic potential. *Curr Med Chem*. 2009;16(10):1248-1265. doi:10.2174/092986709787846640
23. Roxo C, Kotkowiak W, Pasternak A. G-quadruplex-forming aptamers—characteristics, applications, and perspectives. *Molecules*. 2019;24(20):3781. doi:10.3390/MOLECULES24203781

24. Hays EM, Duan W, Shigdar S. Aptamers and glioblastoma: their potential use for imaging and therapeutic applications. *Int J Mol Sci*. 2017;18(12):2576. doi:10.3390/IJMS18122576
25. Visser NFC, Heck AJR. Surface plasmon resonance mass spectrometry in proteomics. *Expert Rev Proteomics*. 2014;5(3):425-433. doi:10.1586/14789450.5.3.425
26. Homola J. Surface plasmon resonance sensors for detection of chemical and biological species. *Chem Rev*. 2008;108(2):462-493. doi:10.1021/cr068107d
27. Ritzefeld M, Sewald N. Real-time analysis of specific protein-DNA interactions with surface plasmon resonance. *J Amino Acids*. 2012;2012:1-19. doi:10.1155/2012/816032
28. Zhang N, Chen Z, Liu D, et al. Structural biology for the molecular insight between aptamers and target proteins. *Int J Mol Sci*. 2021;22(8):4093. doi:10.3390/IJMS22084093
29. Cai S, Yan J, Xiong H, Liu Y, Peng D, Liu Z. Investigations on the interface of nucleic acid aptamers and binding targets. *Analyst*. 2018;143(22):5317-5338. doi:10.1039/C8AN01467A
30. Chen Z, Luo H, Gubu A, et al. Chemically modified aptamers for improving binding affinity to the target proteins via enhanced noncovalent bonding. *Front Cell Dev Biol*. 2023;11:1091809. doi:10.3389/FCELL.2023.1091809/BIBTEX
31. Araujo-Rocha M, Piro B, Noël V, Barbault F. Computational studies of a DNA-based Aptasensor: toward theory-driven transduction improvement. *J Phys Chem B*. 2021;125(33):9499-9506. doi:10.1021/ACS.JPCB.1C05341/ASSET/IMAGES/LARGE/JP1C05341_0007.JPEG
32. Förster U, Weigand JE, Trojanowski P, Suess B, Wachtveitl J. Conformational dynamics of the tetracycline-binding aptamer. *Nucleic Acids Res*. 2012;40(4):1807-1817. doi:10.1093/NAR/GKR835
33. Da Costa JB, Andreiev AI, Dieckmann T. Thermodynamics and kinetics of adaptive binding in the malachite green RNA aptamer. *Biochemistry*. 2013;52(38):6575-6583. doi:10.1021/BI400549S/SUPPL_FILE/BI400549S_SI_001.PDF
34. Costa D, Garrain PA, Baaden M. Understanding small biomolecule-biomaterial interactions: a review of fundamental theoretical and experimental approaches for biomolecule interactions with inorganic surfaces. *J Biomed Mater Res A*. 2013;101A(4):1210-1222. doi:10.1002/JBM.A.34416
35. Ozboyaci M, Kokh DB, Corni S, Wade RC. Modeling and simulation of protein–surface interactions: achievements and challenges. *Q Rev Biophys*. 2016;49:e4. doi:10.1017/S0033583515000256
36. Zahraee H, Arab SS, Khoshbin Z, Bozorgmehr MR. A comprehensive computer simulation insight into inhibitory mechanisms of EGCG and NQTrp ligands on amyloid-beta assemblies as the Alzheimer's disease insignia. *J Biomol Struct Dyn*. 2023;41(20):10830-10839. doi:10.1080/07391102.2022.2158939
37. Plattner N, Doerr S, De Fabritiis G, Noé F. Complete protein–protein association kinetics in atomic detail revealed by molecular dynamics simulations and Markov modelling. *Nat Chem*. 2017;9(10):1005-1011. doi:10.1038/nchem.2785
38. Phanchai W, Srikulwong U, Chompoosor A, Sakonsinsiri C, Puangmali T. Insight into the molecular mechanisms of AuNP-based Aptasensor for colorimetric detection: a molecular dynamics approach. *Langmuir*. 2018;34(21):6161-6169. doi:10.1021/ACS.LANGMUIR.8B00701/ASSET/IMAGES/LARGE/LA-2018-00701E_0008.JPEG
39. Mary V, Haris P, Varghese MK, Aparna P, Sudarsanakumar C. Experimental probing and molecular dynamics simulation of the molecular recognition of DNA duplexes by the flavonoid luteolin. *J Chem Inf Model*. 2017;57(9):2237-2249. doi:10.1021/ACS.JCIM.6B00747/ASSET/IMAGES/LARGE/CI-2016-00747H_0013.JPEG
40. Aho N, Buslaev P, Jansen A, Bauer P, Groenhof G, Hess B. Scalable constant pH molecular dynamics in GROMACS. *J Chem Theory Comput*. 2022;18(10):6148-6160. doi:10.1021/ACS.JCTC.2C00516/SUPPL_FILE/CT2C00516_SI_002.ZIP
41. Wijesinghe KM, Sabbih G, Algama CH, Syed R, Danquah MK, Dhakal S. FRET-based single-molecule detection of pathogen protein IsdA using computationally selected aptamers. *Anal Chem*. 2023;95(26):9839-9846. doi:10.1021/ACS.ANALCHEM.3C00717/ASSET/IMAGES/LARGE/AC3C00717_0006.JPEG
42. Sabbih GO, Wijesinghe KM, Algama C, Dhakal S, Danquah MK. Computational generation and characterization of IsdA-binding aptamers with single-molecule FRET analysis. *Biotechnol J*. 2023;18:2300076. doi:10.1002/BIOT.202300076
43. Allen MP, Tildesley DJ. Computer simulation of liquids: second edition. *Comp Simulat Liquids: Second Edition*. 2017;1-626. doi:10.1093/oso/9780198803195.001.0001
44. Ertekin A, Nussinov R, Haliloglu T. Association of putative concave protein-binding sites with the fluctuation behavior of residues. *Protein Sci*. 2006;15:2265-2277. doi:10.1110/ps.051815006
45. Dumetz AC, Chockla AM, Kaler EW, Lenhoff AM. Effects of pH on protein–protein interactions and implications for protein phase behavior. *Bioch Biophys Acta (BBA) – Protein Proteom*. 2008;1784(4):600-610. doi:10.1016/J.BBAPAP.2007.12.016
46. Yuan H, Wu X, Ren X, et al. Mechanism of pH influence on aptamer binding with Cd 2+ revealed by molecular dynamics simulation. *New J Chem*. 2023;47(19):9239-9249. doi:10.1039/D2NJ06122H
47. Sun L, Shen K, Zhang J, et al. Aptamer based surface plasma resonance assay for direct detection of neuron specific enolase and progastrin-releasing peptide (31-98). *RSC Adv*. 2021;11(51):32135-32142. doi:10.1039/D1RA05041A
48. Agmo Hernández V. An overview of surface forces and the DLVO theory. *ChemTexts*. 2023;9:10. doi:10.1007/s40828-023-00182-9
49. Neves MAD, Slavkovic S, Churcher ZR, Johnson PE. Salt-mediated two-site ligand binding by the cocaine-binding aptamer. *Nucleic Acids Res*. 2017;45(3):1041-1048. doi:10.1093/NAR/GKW1294
50. Otzen DE. Protein unfolding in detergents: effect of micelle structure, ionic strength, pH, and temperature. *Biophys J*. 2002;83:2219-2230. doi:10.1016/S0006-3495(02)73982-9

How to cite this article: Bruce-Tagoe TA, Harnish MT, Soleimani S, Ullah N, Shen T, Danquah MK. Surface plasmon resonance aptasensing and computational analysis of *Staphylococcus aureus* IsdA surface protein. *Biotechnol. Prog.* 2024;40(5):e3475. doi:10.1002/btpr.3475